Effects of plate stiffness on the fatigue resistance and failure location of pipe-to-plate welded joints under bending. Experiments and analysis by nominal and local stress based methods

Leonardo Bertini, Francesco Frendo*, Giuseppe Marulo

Department of Civil and industrial Engineering, Largo Lucio Lazzarino, 56122 Pisa, Italy

Abstract

A series of tests have been carried out using specimens made of a tube, having a thickness of $t = 10$ mm, joined to a plate by fillet welding. Two different kinds of specimen were employed, differing in the plate geometry (stiffness). Both kinds of specimen were tested under bending (prevalent load) and shear loading in as welded conditions.

Different initiation regions for the fatigue cracks were found and significantly different fatigue resistances were obtained for the two geometries in terms of the nominal stress approach (or in terms of applied load vs cycles to failure). Two local methods for the fatigue life assessment were then applied to independently analyse the experimental results: the fictitious notch rounding approach proposed by Radaj, which is also recommended by some international standards and the more recently proposed peak stress method, which is based on the NSIF concept.

It is shown that the nominal stress method, which is by far the simplest method among those recommended in standards for analysing the joint under study, fails to explain the observed different endurances. On the other side, the methods based on local stresses account for the different joint stiffness and provide a reduced scatter in the results. However, even if local approaches, accounts for differences in the structural behaviour of the joint, the knowledge of the actual geometry of the weld need to be accounted for, in order to be able to identify the fatigue crack initiation region.

For a design purpose, a safe prediction of the fatigue endurance of the joint can be obtained by all the analysed methods, if the corresponding recommended design curve is used.

Keywords: Fatigue strength, Welded joints, Steel, Fictitious notch radius, Peak stress

1. Introduction

The fatigue life assessment of welded joints is still an open and debated subject. One of the main features of the welding process is that localized high temperatures are reached and, as a consequence, the material microstructure (i.e. grain size, secondary phases, microstructural defects etc.) and the mechanical properties (e.g. yield strength, hardness etc.) in the fused zone and in the heat affected zone are modified. Some micro and macro geometric discontinuities (such as e.g. inclusions, porosity, undercutting) may also be introduced by the welding process itself and high residual stresses are generated in proximity of the weld seam. The variability typical of the welding process when combined with the localised nature of damage initiation, usually, gives raise to relevant scatter in fatigue test's data. For these reasons the fatigue assessment of welded joints is complex and different analysis methods have been proposed in standards [1, 2, 3, 4] and, more generally, in the technical literature (see e.g. [5, 6, 7, 8, 9, 10, 11, 12, 13, 14, 15]).

Dealing with welded joints, there are different potential regions where the fatigue crack responsible of the final failure may initiate, namely the weld root and the weld toe. Despite of that, some of the methods that are recommended in standards, such as the nominal stress approach, does not consider the local geometry of the weld and, consequently, do not differentiate on the initiation region. In addition, some of the proposed local methods, such as the hot spot (or structural stress) method, only consider the case of failures from the weld toe. To this regard, it is also infrequent that papers available in the technical literature from different authors report different initiation regions for the same kind of specimen, material and loading conditions (see e.g. [16, 17, 18, 19, 20]).

In the present work the effect of the plate geometry on the fatigue crack initiation region and on the observed fatigue endurance in a frequently employed welded joint, i.e. the pipe-to-plate joint, is discussed. For this reason a dedicated experimental campaign was conducted, extending the database of experimental results already presented in previous works by the authors [16, 21]. The newly employed specimens differ from the previous ones in terms of plate stiffness (Fig. 1). However, if the nominal stress method is considered, the specimens belong to the same structural detail (see [1, 2]).

The fatigue strength of the analysed flange-tube welded joints has been discussed in [17, 18, 19], for the case of fillet-

*Corresponding author: Tel.:+39(0)502218074; fax:+30(0)502210604
E-mail address: francesco.frendo@unipi.it

welded joints is and in [7, 9, 20] for the case of bevel butt welded joint. However, in none of those works the stiffness of the plate is explicitly regarded as a significant parameter in terms of the fatigue strength of the joint.

The discussion of the results is based on three endurable stresses obtained by different analysis methods, i.e. the nominal stress approach, which is by far the most simple and used method when applicable, and two local stress methods: the already well established fictitious notch rounding radius [22, 23, 24] and the more recently proposed peak stress methods [25, 26]. The capability of the different methods, which are based on quite different theoretical background, in interpreting the experimental endurances is also discussed in terms of scatter band and prediction of the crack initiation region.

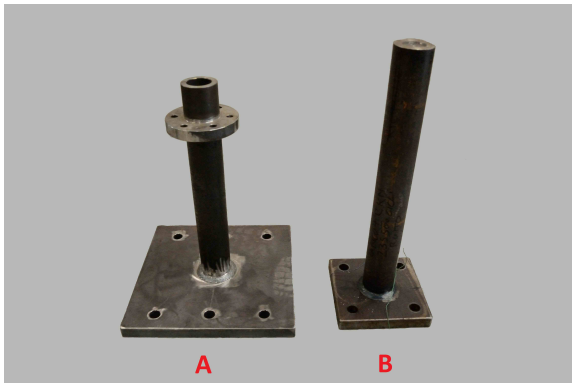

Figure 1: Tested specimens. Type A specimen with the larger plate (on the left) and type B specimen with the smaller plate (on the right).

2. Evaluation of the fatigue strength of welded joints by the nominal stress, the fictitious notch rounding radius and the peak stress method

In this work both global and local methods have been used for the fatigue assessment. The nominal stress method ([2]) belongs to the former category and, if a nominal stress can be defined, is by far the most simple and most widely used method. For this reason it is also referenced in standards [1] and is the usually preferred method for engineers working in the industry. Furthermore two local methods have been used: the notch stress method (see e.g. [2] and [23]) and the peak stress method ([25]). A brief review on their theoretical background is presented in the following.

It is worth to note that both the local methods here reviewed assumes a sharp V notch with a null tip radius at the most solicited region, i.e. weld toe or root. This is a widely used assumption for design purposes, since it is a conservative hypothesis and, in addition, is an easy way to bypass the difficulties related to the evaluation of the actual notch tip radius.

2.1. Nominal stress method

This method is recommended by both the *International Institute if Welding* (IIW) [2] and by the Eurocode 3 [1]. According to this method, the nominal stress on the weld section is calculated according to common stress formulas, based on beam theory. In the present case, due to the length of the tube, the applied load results in a prevalent bending component at the weld critical section. Therefore, the nominal stress can be evaluated by equation 1, where M_b is the bending moment, W_x is the strength modulus of the weld section, which is defined with reference to the weld throat size.

$$\sigma_n = \frac{M_b}{W_x} \tag{1}$$

It is worth noting that only nominal dimensions of the weld seam (weld throat) are taken into the calculation and there is no account for the actual joint geometry, meaning that the effect of all the fatigue relevant parameters should be included in the fatigue class of the structural detail [27]. It can be easily understood that, by using this method, the fatigue life assessment is as reliable as the structural detail is similar to one of the details covered by the code. In the present case both the test specimens A and B (Fig. 1) can be referred to structural detail number 423 as classified by [2], with no distinction.

2.2. Fictitious notch rounding radius

Fatigue assessment through the use of a fictitious notch radius was developed by Neuber [28] based on the idea of averaging the linear elastic stress over the micro-structural length in the ligament of the notch.

$$\overline{\sigma} = \frac{1}{\rho^*} \int_0^{\rho^*} \sigma(x) dx. \tag{2}$$

The average stress ($\overline{\sigma}$) is used as a fatigue effective stress. Due to limitations in numerical calculation methods at that time, Neuber formulated the procedure of fictitious notch rounding, where the averaged stress on the actual notch with a radius ρ is substituted by the maximum stress on a fictitiously enlarged notch radius, termed ρ_f in eq. 3. Here the support factor (s) is an analytically derived factor that depends on the stress state at the notch tip and on the failure hypothesis (see e.g. [29, 30]).

$$\rho_f = \rho + s\rho^* \tag{3}$$

For welded joints, Radaj [23] assumed the notch to be V-shaped with tip radius equal to zero ($\rho = 0$), which is always a conservative hypothesis. He also obtained $s = 2.5$ and the micro-support length $\rho^* = 0.4$ for steel. Then, the fictitious radius resulted $\rho_f = 1$ mm, which is called reference radius.

This procedure has been successfully applied for decades in the fatigue life assessment of joints with a thickness $t \geq 5$ mm and is one of the methods recommended by the *International Institute of Welding* (IIW) [2].

2.3. Peak stress method

The peak stress method (PSM) was originally proposed by Nisitani et al. [31] for notched specimens. More recently Meneghetti et al. have proposed its use also for the fatigue life

assessment of welded joints [25, 26] and have extended its application in case of three dimensional problems.

$$\Delta\sigma_{eq,peak} = \sqrt{f_{w1}^2 \Delta\sigma_{\theta\theta,\theta=0,peak}^2 + f_{w2}^2 \Delta\tau_{r\theta,\theta=0,peak}^2}; \quad (4)$$

The basic idea behind the PSM is to estimate the stress intensity factor (NSIF) with a Finite Element (FE) model, which is characterized by a coarse free mesh. Also in this case the notches are assumed to be V-shaped with a null tip radius. The mode I and II elastic stresses obtained from such model are then linked to the desired NSIFs by the simple equation 4. In that equation, $\Delta\sigma_{\theta\theta,\theta=0,peak}$ and $\Delta\tau_{r\theta,\theta=0,peak}$ are the mode I and mode II stresses obtained from the FE model, while f_{w1} and f_{w2} are empirical coefficients related to the averaged element size adopted in the model.

The main advantage of the PSM is the great simplicity of the FE model which is needed to obtain the peak stress values. In the present work the mesh of the weld seam was composed of first order elements directly generated by the free meshing tool of the Ansys program on the basis of the user defined average element size. The mesh can be coarser compared to that required to evaluate directly the NSIF or the notch stress on the fictitious radius.

This method is not included in any deign code due to its recent formulation. However, it has already been successfully applied to a wide range of experimental data [25].

3. Experimental setup

The tested specimens were designed in order to reproduce a plate-to-tube joint typically found in railway boogie components. The tube had an external diameter of $d = 64$ mm and a thickness of $t_t = 10$ mm, while the basic thickness of the plate was $t_p = 25$ mm. All the specimens were made of S355JR, a common structural steel, for which $\sigma_y = 360$ MPa and $\sigma_u = 520$ MPa. The thickness of the plate in the joint region was reduced, to be kept closer to that of the pipe. The pipe was joined to the plate by wire welding by using a 1.2 mm diameter ER70S-6 wire, having 460 MPa yield strength and 570 MPa tensile strength; the current and tension of the welding apparatus were set to 215 A and 24.5 V, respectively.

Two kinds of specimen have been tested (Fig. 1), differing in the geometry of the plate, particularly as regards the welded joint region. All the specimens were tested in as welded condition.

With reference to Fig. 2, the main difference between the two types of specimen was the radius ϕ_a and the depth h of the central counterbore, which were chosen in order to produce significant differences in plate thickness in the joint region. In case of type A specimens the plate width was $L = 330$ mm and the distance between the supports was $i = 250$ mm. On the other side, for type B specimens those dimensions were $L = 186$ mm and $i = 125$ mm, respectively. Furthermore, a counterbore was machined in both plates in order to reduce the plate thickness locally and to install the pressure air tube for crack detection (see Fig. 2). The dimensions of this counterbore were $\phi_a = 140$ mm

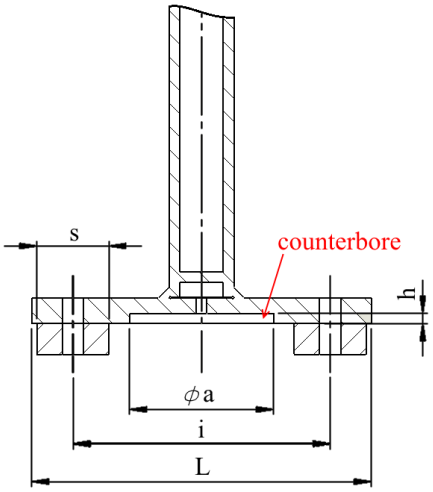

Figure 2: Specimen geometry definition.

and $h = 10$ mm for type A specimens and $\phi_a = 80$ mm and $h = 5$ mm for type B specimens. In both cases the width of the supports was $s = 70$ mm. The specimens were fixed to the bench by bolts: six M14 and four M20 bolts were employed for type A and type B specimens, respectively (see also Fig. 1).

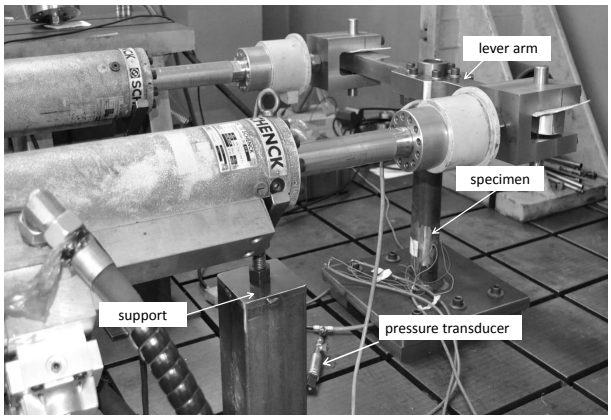

Figure 3: Loading apparatus. The specimen is loaded by two hydraulic actuators attached at the extremities of a lever arm; this test rig was developed to have the possibility of applying combined bending and torsion ([21]).

Both specimens were tested under constant amplitude loading, with a load ratio of $R = -1$ and $R = 0$. The external load is equivalent to a force applied on the top of the tube, which produces bending and shear stresses in the welded cross section (see Fig. 3). However, the shear stress was negligible compared to the bending one, due to the length of the tube (375 mm for type A and 510 mm for type B specimens).

The adopted failure criterion was the presence of a through the thickness crack, or the pipe displacement to exceed a predefined value. The occurrence of a through crack was easily detected by the sudden drop in air pressure imposed in the lower

chamber trough a hole in the counterbore at the start of the test. As an alternative condition, in case of failure through the plate. i.e. crack type 1 (see next section), the test was also stopped if the actuators displacement exceeded a predefined threshold.

4. Cracks initiation regions and crack paths

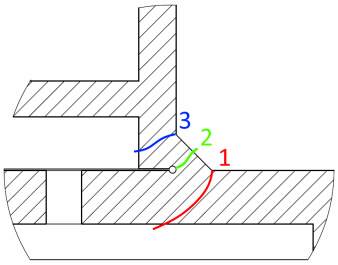

Figure 4: Observed crack paths.

For the analysed pipe-to-plate joint three main candidate initiation points and corresponding crack paths can be identified depending on the joint behaviour under the applied load: crack through the plate thickness originated at the weld toe on the flange (Fig.4, path 1), crack through the seam weld originated at the weld root (Fig.4, path 2) and crack through the pipe wall originated at the weld toe on the tube (Fig.4, path 3).

For type A specimens (Fig. 5), cracks starting from the weld toe on the flange (i.e. path 1) were always observed. In some cases, cracks emanating from the weld root (i.e. path 2) were also observed, which were presumably initiated in a second phase, due to the stress increase in that region, following the cross section reduction produced by the growth of path 1 crack. It has also to be considered that in case of a path 1 crack only the plate is damaged and no crack is detected by the employed detection method (i.e. no pressure drop occurs). In this cases tests were stopped when the limit on the displacement of the hydraulic actuators was reached. This limit was set to a few millimetres beyond the maximum displacement at the maximum applied load and can be produced by a relatively large defect, with respect to the minimum detectable defect that produced a drop in the air pressure.

For type B specimens (Fig. 6), the failure was caused by crack originated from the weld root (i.e. path 2 crack) or, less frequently, from the weld toe on the tube (i.e. path 3 crack).

5. Results in terms of nominal stresses

The nominal stress for bending is easily calculated by Eq.1. It is worth to note that the strength modulus is a function of the weld seam geometry and is not influenced by the plate geometry. For this method there is no distinction between type A and type B specimens.

The results obtained by this method, as S–N curves for $R = -1$ and $R = 0$ respectively, are given in Fig. 7 and Fig. 8. The

Figure 5: Typical fracture surface of a type A specimen. A very long and extensive crack propagated in the plate (for the specimen shown in the figure, the propagation was intentionally prolonged), without causing any pressure drop.

Figure 6: Fractured type B specimen. The dominant crack was originated at the weld root. A secondary crack, that originated from the weld toe on the tube, can also be recognized.

reference IIW design curve for this structural detail [2] is also shown for comparison in both graphs.

It can be observed that, for any stress amplitude, type B specimens had a significantly greater endurance compared to type A specimens. This is more evident for the tests with the load ratio $R = -1$.

At the same time it can be observed that all the tests are on the safe side of the design curve; this is not surprising since the design curve is referred to 97,7% probability of survival.

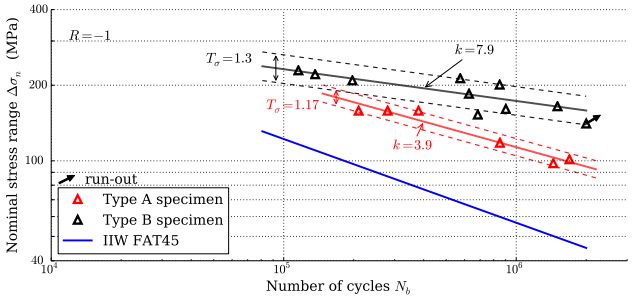

Figure 7: Results for type A and type B specimens in terms of nominal stresses. S–N curve for bending and load ratio $R = -1$.

6. Finite element modelling of the test

In both the notch stress and the peak stress methods the endurable stress is obtained from an elastic FE analysis.

The model of the specimen can be considered as composed of two parts: the weld seam and the whole experimental setup

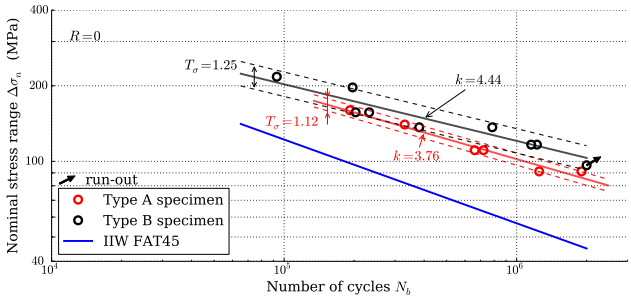

Figure 8: Results for type A and type B specimens in terms of nominal stresses. S–N curve for bending and load ratio $R = 0$.

composed of the specimen, the constraints and the loading arm. For each one of the mentioned local methods it is possible to find, in the technical literature, specific instructions on how to model the weld seam. On the other side, the global structure of the model is not dependent on the local method used and only needs to accurately reproduce the test geometry. The residual stress state resulting from the welding process was not included in the FE analyses. Accordingly, the design curves given in all the plots are referred to the as welded condition.

6.1. Weld seam model

For the notch stress method, following [2], the value of $\rho_f = 1$ mm was selected as for joints with a thickness $t > 5$ mm. Details of the mesh of the weld seam were defined according to the instructions given in [32]. A mapped mesh (Fig. 9) was created in the notch areas, placing 24 elements over 360° on each fictitious rounding. Furthermore a shape factor $V = 2$ was imposed (this represents the ratio between the circumferential and radial dimensions of the elements). Second order brick elements having 20 nodes were employed (*brick186* from *ANSYS* ® library). According to the cited paper, this kind of mesh guarantees an error below 2% on the computed elastic stresses.

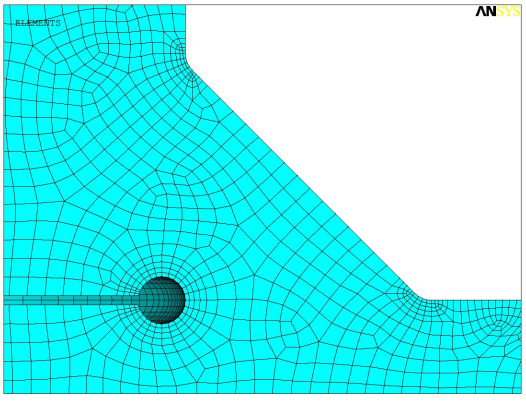

Figure 9: Weld seam model for the application of the fictitious notch stress method.

The requirements for the weld seam FE model in relation to the peak stress method are defined in [25, 26]. In this case the notches are modelled as sharp (i.e. zero tip radius) and the weld seam area is meshed by the free meshing tool of the software imposing an average element size $d = 1$ mm (Fig. 10). In this case, first order brick elements with 8 nodes were used (*brick185* from *ANSYS* ® library). At the weld root an opening angle $2\alpha = 0$ is present; the two lines of the V-shaped in the FE model are overlapped and cannot be distinguished (Fig. 10).

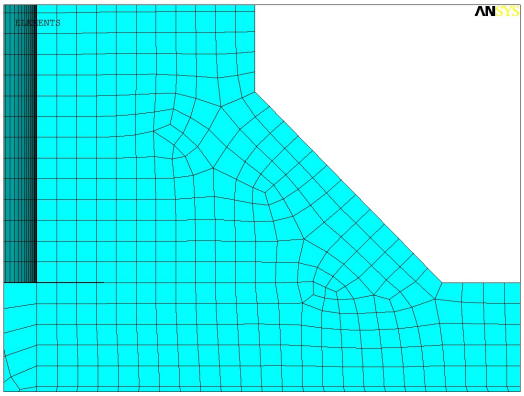

Figure 10: Weld seam model for the application of the peak stress method.

We can notice that the peak stress method is much easier to be implemented on the FE software. In addition, its computational effort is smaller, due the use of first order elements.

6.2. Global model of the test and its experimental validation

The detailed 3D model of the test shown in Fig. 11 was developed. A linear elastic material (steel with elastic modulus and Poisson's ratio $E = 210$ GPa and $\nu = 0.3$, respectively) was considered for both the pipe and the plate.

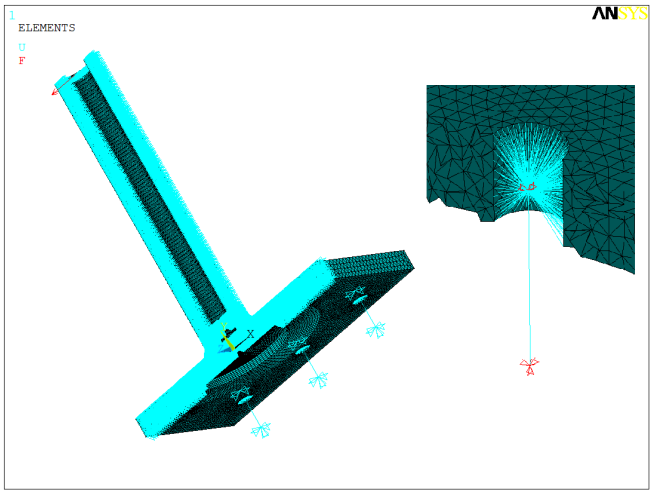

Figure 11: 3D model in case of type A specimen geometry. A similar model was also developed for type B specimens.

Thanks to the symmetry about the bending plane only half of the specimen was modelled. The actual plate geometry and the elasticity of the bolts were included. The bolts were reproduced as links with proper length and cross sections and were constrained to the specimen (internal surface of the holes) by

a spider of rigid (i.e. having very high stiffness) links. In addition, the lower node of the links representing the bolts were fully constrained, while the upper nodes were constrained along the plane directions of the lower plate of the specimen, leaving only the possibility to move in a direction orthogonal to the plate.

Type A and type B specimens differ from each other in the dimensions of the plate and this turned out to be determinant for the failure mode, among those discussed in section 4. Since the elastic stresses at the notches were recognized as a determinant aspect, an experimental validation of the FE model was planned for one of the specimens. A series of 12 strain gauges was applied in the bending plane (radial direction with reference to the pipe) on the plate of a type A specimen, in the surrounding of the seam weld (see Fig 12). This allowed to measure a component of the strain field near the weld area and to compare it to the numerical results obtained by the FE model.

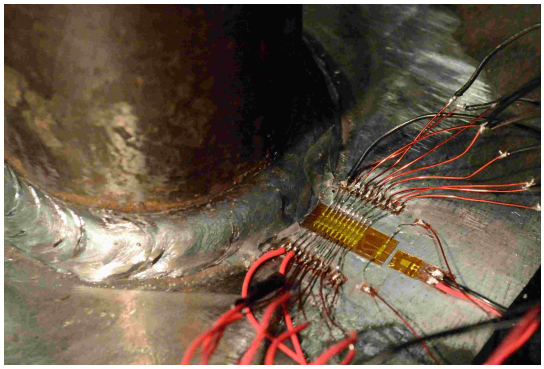

Figure 12: Strain gages placed on the plate of a type A specimen, nearby the the seam weld.

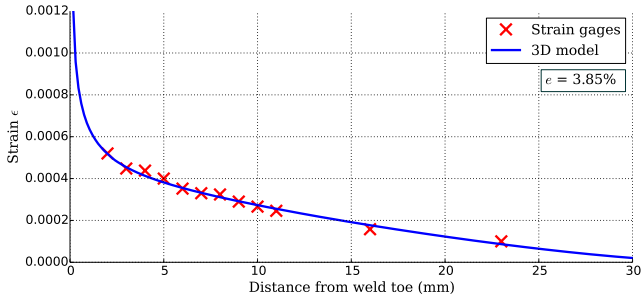

Figure 13: Strains of the plate along a radial path (distances from the weld toe). Comparison between the values obtained from strain gages measurements and from the developed FE models.

The twelve gages were placed with distances from the (nominal) weld toe between $d_1 = 2$ mm (for the first strain gauge) and $d_{12} = 23$ mm (for the last strain gauge). Those distance values are very close to the ones recommended in order to evaluate the structural stress, which is the representative stress parameter of the Hot–Spot method [2]. Accordingly, it can be reasonably considered that the so-measured strains are not related to the local weld seam geometry.

A comparison between experimental and numerical strain is given in Fig. 13. It was verified that the strains had a linear dependence on the load level. The plots refer to a bending load of $M_f = 1875$ Nm acting in the critical cross section. As it can be observed the 3D model with a correct reproduction of the plate geometry and constraining system resulted to be in rather good agreement with the experimental results. The average relative error, obtained for the 12 strain gauges, between experimental and numerical strain is also given in the plot.

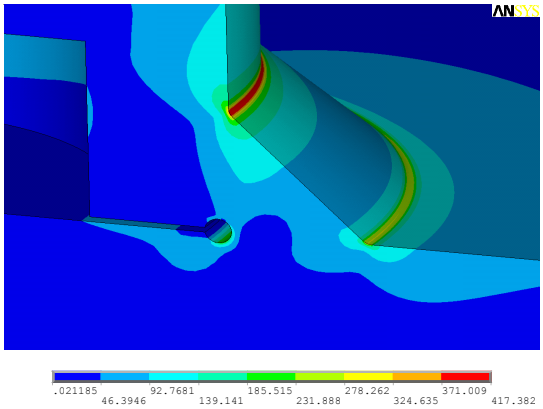

Figure 14: Notch stress method and type A specimen.

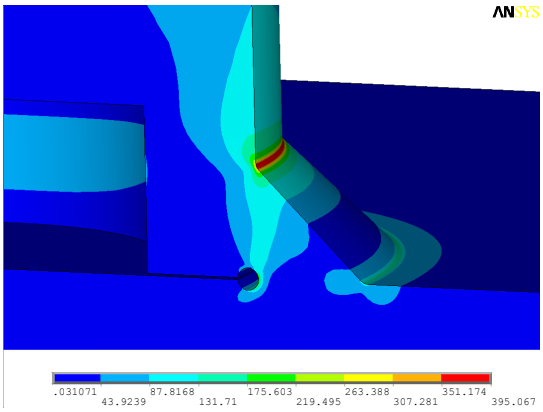

Figure 15: Notch stress method and type B specimen.

7. Durability analysis based on the notch stress concept and the peak stress method

The following Figs.14, 15, 16 and 17 show the von Mises equivalent stress for type A and type B specimens, obtained by the fictitious notch stress and the peak stress methods.

Even if the two methods use a different endurable stress, it is possible to say that in all four cases for the FE model, the crack nucleation region is at the weld toe on the tube side, i.e. crack type 3 in Fig.4. This did not correspond to the experimental evidences described in Sec. 4. In particular, for type A specimens, cracks in this location were never observed.

Starting from the stress field obtained from the FE models, the endurable stress of the two local methods was determined.

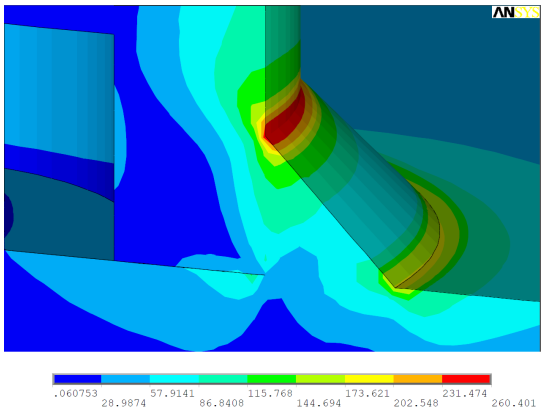

Figure 16: Peak stress method and type A specimen.

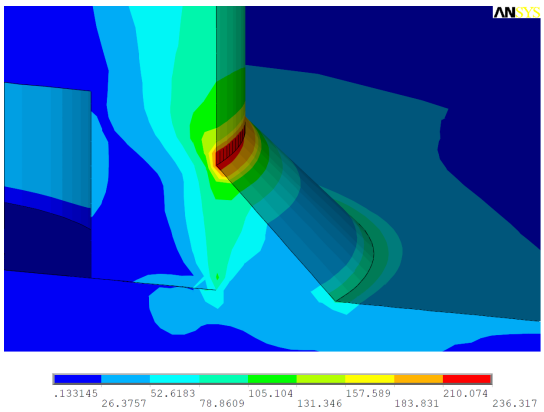

Figure 17: Peak stress method and type B specimen.

For the notch stress method this is quite straightforward, since in this case the fatigue strength is assumed to be related to the von Mises equivalent stress range at the most stressed point of the fictitiously introduced radius. Instead, for the peak stress method the mode I and mode II elastic stresses have to be extracted from the FE model. Those values are then combined together, through appropriate factors in order to obtain the equivalent peak stress $\Delta\sigma_{eq,peak}$ (see Eq.4). In the present work only the mode I stresses have been computed, the other being negligible.

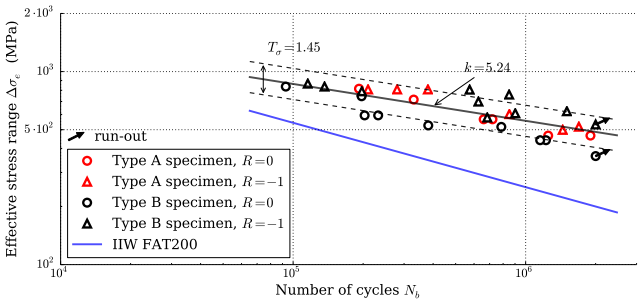

Figure 18: Effective stress range vs Number of cycles to failure for the notch stress method.

The obtained S–N curves are given in Figs. 18 and 19 together with the appropriate design reference curve. For the notch stress method the FAT 200 with a slope coefficient $k = 3$ was selected, having chosen the von Mises equivalent stress hypothesis and a fictitious radius $\rho_f = 1$ mm [2]. This design curve is related to a survival probability of $P_s = 97,7\%$.

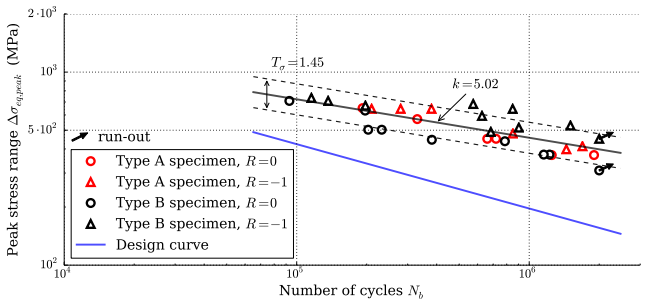

Figure 19: Equivalent peak stress range vs Number of cycles to failure for the peak stress method.

In a similar way, for the peak stress method the curve given in [25, 26] for a survival probability of $P_s = 97,7\%$ was considered. This curve has a slope coefficient $k = 3$ and a value of $\Delta\sigma_{\text{eq,peak}} = 156$ MPa at $2 \cdot 10^6$ cycles.

Even if the two plots cannot be directly compared, it is interesting to observe that, by using a local approach, the two specimen types do not show any relevant difference in terms of endurance vs. effective or peak stress range, as they did when the nominal stresses were taken as reference (see previous Fig. 7 and Fig. 8). This improvement was caused by the fact that, in order to properly evaluate the local stresses, the stiffness of the plate had to be correctly evaluated. Going from the nominal stress reference to the local stress reference, a great reduction of the scatter band is produced, as well. In addition, it can be observed that all the experimental points are on the safe side with respect to the suggested reference curve.

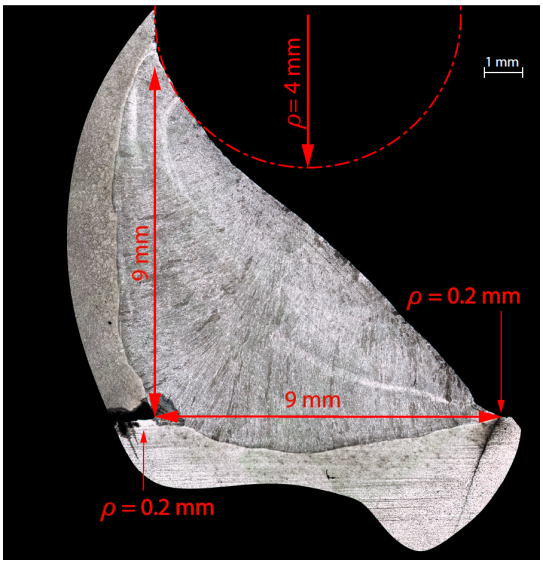

Figure 20: Weld seam section, type A specimens.

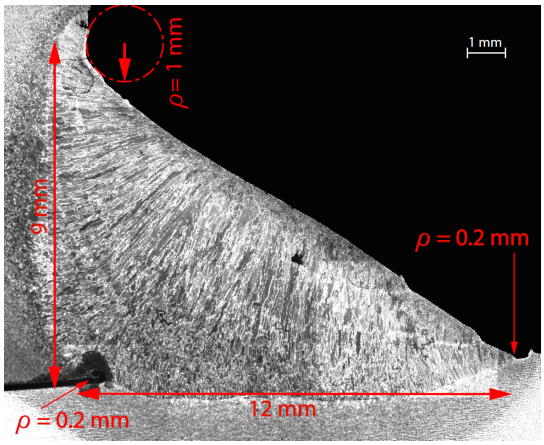

Figure 21: Weld seam section, type B specimens.

8. Stress analysis based on the actual seam weld geometry

In previous section it was shown that local methods, accounting for the actual joint stiffness, allowed to avoid the apparent discrepancies given by the nominal stress method when comparing the results obtained by type A and type B specimens. However, it was found that both local methods failed in the prediction of the fatigue crack initiation region.

In order to explain those evidences and to investigate more in depth this aspect, the actual geometry of the seam weld was evaluated on the basis of several pictures of cross-sections that were cut from both type A and type B specimens (see e.g. Figs. 20 and 21).

Even if the same nominal dimensions were requested, the actual geometry of the seam welds showed some differences. In particular, it can be observed that the notch on the tube side has a bigger tip radius compared the others. The difference in the two radii could be explained based on the weld position. As reported in [33] in fillet welds the fused material shows a tendency to float downwards before solidification under the effect of gravity. In the cited paper it is described how the upper toe (i.e. tube side toe) tends to have a bigger radius compared to the lower toe (i.e. plate side toe), thus resulting less critical for the fatigue endurance.

Therefore, the worst case of a null notch tip radius when applied to the tube side toe is very conservative and the stress state in this region is overestimated by that hypothesis. This can explain why no cracks were detected in this location during experimental tests, oppositely to what predicted by the used local methods.

A FE model based on the average actual geometry was then setup. Five geometric parameters were selected to represent the actual geometry of the seam weld: the tip radius of three notches, the height and the width of the seam. These parameters were measured on ten sections taken from each specimen type. The resulting average values are given in Figs. 20 and 21.

Three dimensional FE models of the type A and type B specimens were then developed, according to what described in Sec. 6.2, based on the so determined average geometries . In order to achieve a fairly good estimation of the elastic stress in the weld area, the notches were modelled by using a mapped mesh and second order elements, similarly to what previously described for the notch stress method (see Sec. 6.1).

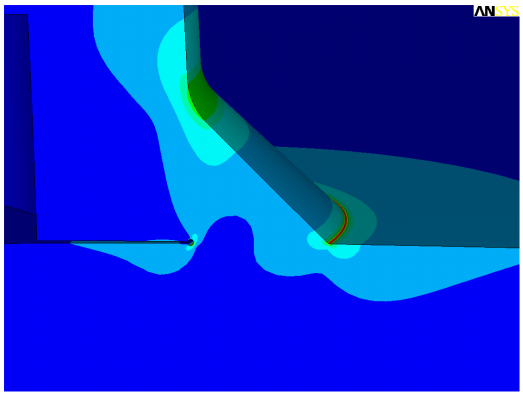

Figure 22: FE model for the actual geometry of type A specimens.

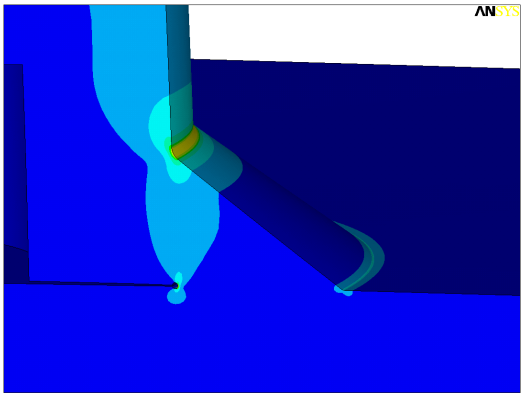

Figure 23: FE model for the actual geometry of type B specimens.

The von Mises equivalent stress field is plotted in Figs. 22 and 23, for the type A and type B specimens, respectively, for a bending load of $M_f = 1875$ Nm acting in the critical cross section.

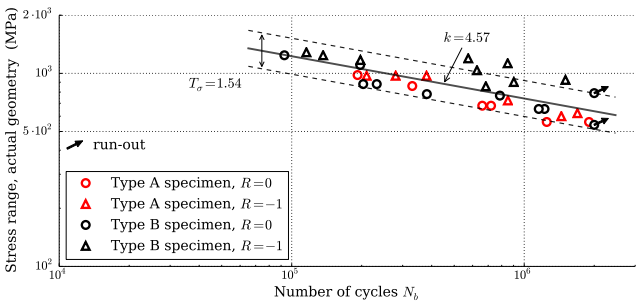

Figure 24: S–N data obtained considering the maximun von Mises stress and the actual weld geometry.

Figure 24 shows the S–N data obtained considering the peak value of the equivalent von Mises stress, which is located at the

weld toe on the plate and at the weld root for type A and type B specimens, respectively.

Table 1 and 2 shows the peak value (data for $\rho^* = 0$) of the von Mises equivalent stress together with the average values obtained considering four different micro-support distances (i.e. from $\rho^* = 0.1$ mm to $\rho^* = 0.4$ mm) along a path oriented in the radial direction and starting from the point where the maximum local stress was obtained. The average stress is recognized as a more representative parameter than the peak stress for fatigue cracks initiation. The averaged values were obtained integrating the von Mises equivalent stress as per Eq. 2 over the given micro-support distances (i.e. ρ^*).

Type A Specimen			
ρ^*	root	tube side toe	plate side toe
0	460	270	500
0.1	276	258	302
0.2	196	248	237
0.3	153	238	203
0.4	127	230	182

Table 1: Values of the von Mises stress (MPa). Maximum and averaged values over a micro-support distance ranging from $\rho^* = 0.1$ mm to $\rho^* = 0.4$ mm in case of type A specimens.

Type B Specimen			
ρ^*	root	tube side toe	plate side toe
0	564	428	190
0.1	339	371	114
0.2	243	328	92
0.3	193	295	80
0.4	162	270	73

Table 2: Values of the von Mises stress (MPa). Maximum and averaged values over a micro-support distance from $\rho^* = 0.1$ mm to $\rho^* = 0.4$ mm in case of type B specimens.

If we consider the maximum von Mises stress over the three notches (weld root, weld toe on the tube and weld toe on the plate), i.e. the value for $\rho^* = 0$ mm, it can be concluded that these FE models, based on the actual weld geometries are capable of predicting the correct initiation point of fatigue cracks for both type A and type B specimens.

For type A specimen the model shows that most solicited areas are the weld toe on the plate side and, at a slightly lower extent, the weld root, while the toe on the the tube side appears to be subjected to a significantly lower stress. For type B specimens the model indicates the weld root as the most solicited region and the weld toe on the plate as the notch with the lower stress level.

These numerical results agree with experimental evidence: for type A specimen the great majority of cracks originated from the toe on the plate side, while some crack was sometimes observed starting from the root (Sec. 4); for type B specimen cracks generally started from the weld root and, occasionally, from the weld toe on the tube side

The observation of Tables 1 and 2 showed that this correspondence may be lost as the microsupport distance is allowed to grow over 0.1 mm. This appears as an indication of a very small or null value for this parameter as appropriate, at least in the present case. Further studies are required to analyse this result with reference to other joint geometries and weld shapes.

9. Conclusions

The following conclusions can be drawn from the experimental results and from the numerical analysis:

- experimental results showed that the plate thickness can significantly affect the fatigue strength and the fatigue crack initiation point in a pipe to plate joint subject to bending;
- the predictive method based on nominal stresses was not able to account for the effects of plate thickness on fatigue strength, even if predictions based of IIW or Eurocode 3 recommendations proved to be conservative;
- the use of local methods based on a 3D FE analysis of the joint allowed to properly account for the effects of plate thickness on fatigue strength; in the examined tests, all the results appeared to belong to a single dispersion and its measure T_σ reduced significantly, passing from the nominal stress to the local stress;
- the design curves recommended in standards generally give conservative results, due to the large safety margin provided by the $P_s = 97.7\%$ probability of survival;
- the local methods that were applied (i.e. the fictitious notch radius and the peak stress method) appeared to give very similar results both in terms of scatter and safety margin of the recommended reference S–N curves with respect to the experimentally determined endurances (see Fig. 18 and Fig. 19);
- despite the satisfactory accuracy in predicting fatigue strength, both local methods were not able to individuate the actual failure location for all cases;
- a detailed examination of the weld section shape showed relevant differences between the plate side and the pipe side micro-geometry of the weld toe, which was not accounted for by standard local methods and which was probably responsible of crack nucleation position;
- a FE model accounting for the detailed actual geometry of the weld proved to be able to predict properly the initiation point; the analysis appears to indicate that the correct prediction of the failure location point should account for actual weld geometry, rather than for nominal geometry;
- the analysis shown on the averaged stress obtained for different microsupport distances starting from the FE model based on the actual weld geometries, pointed out that the evaluation of the local endurable stress is a critical step in the fatigue analysis of welded joints;

- as a consequence of the last previous points it can be concluded that any attempt of predicting the failure initiation region by simplified idealized models, e.g. based on the nominal geometry of the weld, may result useless.

Acknowledgements

This work was supported by the University of Pisa under the Institutional Research Grant "PRA"– Project no. PRA_2016_36

References

[1] EN, Eurocode3: design of steel structures. Fatigue.
[2] A. Hobbacher, Fatigue design of welded joints and components: Recommendations of IIW Joint Working Group XIII-XV, Woodhead Publishing, 1996.
[3] C. UNI, 10011steel structures, Instructions of design, construction, testing and maintenance. UNI, Italy.
[4] B. S. BS7910, Guide on methods for assessing the acceptability of flaws in fusion welded structures, British Standards Institutions, London.
[5] D. Radaj, C. M. Sonsino, W. Fricke, Fatigue assessment of welded joints by local approaches, Woodhead Publishing Limited, 2006.
[6] D. Radaj, C. Sonsino, W. Fricke, Recent developments in local concepts of fatigue assessment of welded joints, International Journal of Fatigue 31 (1) (2009) 2–11.
[7] C. Sonsino, S. Maddox, Multiaxial fatigue of welded structures–problems and present solutions, in: Proceedings of the sixth international Conference on Biaxial/Multiaxial fatigue and Fracture, 2001, pp. 3–15.
[8] E. Niemi, Stress determination for fatigue analysis of welded components, Woodhead Publishing, 1995.
[9] C. Sonsino, Multiaxial fatigue assessment of welded joints–recommendations for design codes, International Journal of Fatigue 31 (1) (2009) 173–187.
[10] Y. Verreman, B. Nie, Early development of fatigue cracking at manual fillet welds, Fatigue & Fracture of Engineering Materials & Structures 19 (6) (1996) 669–681.
[11] P. Lazzarin, R. Tovo, A notch intensity factor approach to the stress analysis of welds, Fatigue & fracture of engineering materials & structures 21 (9) (1998) 1089–1103.
[12] P. Livieri, P. Lazzarin, Fatigue strength of steel and aluminium welded joints based on generalised stress intensity factors and local strain energy values, International Journal of Fracture 133 (3) (2005) 247–276.
[13] W. Fricke, Guideline for the fatigue assessment by notch stress analysis for welded structures, International Institute of Welding 13 (2010) 2240–08.
[14] R. Tovo, P. Livieri, An implicit gradient application to fatigue of sharp notches and weldments, Engineering Fracture Mechanics 74 (4) (2007) 515–526.
[15] E. Mikkola, Y. Murakami, G. Marquis, Fatigue life assessment of welded joints by the equivalent crack length method, Procedia Materials Science 3 (2014) 1822–1827.
[16] L. Bertini, A. Cera, F. Frendo, Experimental investigation of the fatigue resistance of pipe-to-plate welded connections under bending, torsion and mixed mode loading, International Journal of Fatigue 68 (2014) 178–185.
[17] A. Siljander, P. Kurath, F. Lawrence, Non-proportional fatigue of welded structures, Advances in fatigue lifetime predictive techniques, ASTM STP 1122 (1992) 319–338.
[18] J.-Y. Yung, F. Lawrence, Predicting the fatigue life of welds under combined bending and torsion, in: ICBMFF2, 2013.
[19] G. Razmjoo, Fatigue of load-carrying fillet welded joints under multiaxial loading, Fatigue: core research from TWI, Woodhead, UK (2000) 63–99.
[20] A. Esderts, J. Willen, M. Kassner, Fatigue strength analysis of welded joints in closed steel sections in rail vehicles, International Journal of Fatigue 34 (1) (2012) 112–121.
[21] F. Frendo, L. Bertini, Fatigue resistance of pipe-to-plate welded joint under in-phase and out-of-phase combined bending and torsion, International Journal of Fatigue 79 (2015) 46–53.
[22] D. Radaj, Design and analysis of fatigue resistant welded structures, Elsevier, 1990.
[23] D. Radaj, M. Vormwald, Generalised neuber concept of fictitious notch rounding, in: Advanced Methods of Fatigue Assessment, Springer, 2013, pp. 1–100.
[24] C. Sonsino, W. Fricke, F. De Bruyne, A. Hoppe, A. Ahmadi, G. Zhang, Notch stress concepts for the fatigue assessment of welded joints–background and applications, International Journal of Fatigue 34 (1) (2012) 2–16.
[25] G. Meneghetti, The peak stress method applied to fatigue assessments of steel and aluminium fillet-welded joints subjected to mode i loading, Fatigue & Fracture of Engineering Materials & Structures 31 (5) (2008) 346–369.
[26] G. Meneghetti, B. Atzori, Il metodo della tensione di picco applicato ad analisi agli elementi finiti tridimensionali per la verifica a fatica di giunti saldati sollecitati a trazione o flessione con rotture al piede o alla radice del cordone, AIAS 2014 - 326.
[27] A. Hobbacher, The new iiw recommendations for fatigue assessment of welded joints and components–a comprehensive code recently updated, International Journal of Fatigue 31 (1) (2009) 50–58.
[28] H. Neuber, Kerbspannungslehre, Vol. 3, Springer-Verlag Berlin, 1985.
[29] F. Berto, P. Lazzarin, D. Radaj, Fictitious notch rounding concept applied to sharp v-notches: Evaluation of the microstructural support factor for different failure hypotheses. part i: Basic stress equations, Engineering Fracture Mechanics 75 (10) (2008) 3060–3072, cited By 39.
[30] F. Berto, P. Lazzarin, D. Radaj, Fictitious notch rounding concept applied to sharp v-notches: Evaluation of the microstructural support factor for different failure hypotheses. part ii: Microstructural support analysis, Engineering Fracture Mechanics 76 (9) (2009) 1151–1175, cited By 48.
[31] H. Nisitani, T. Teranishi, K i of a circumferential crack emanating from an ellipsoidal cavity obtained by the crack tip stress method in fem, Engineering fracture mechanics 71 (4) (2004) 579–585.
[32] J. Baumgartner, T. Bruder, An efficient meshing approach for the calculation of notch stresses, Welding in the World 57 (1) (2013) 137–145.
[33] Z. Barsoum, B. Jonsson, Influence of weld quality on the fatigue strength in seam welds, Engineering Failure Analysis 18 (3) (2011) 971–979.